Measuring the optical responses of core@shell nanowires by using cathodoluminescence spectroscopy

What are the resonances in scattering spectra of $Cu@Cu_2O$ core@shell nanowires of different core-shell dimensions, and how does this compare to theory?

Linda van der Waart
6077560
18-07-2013

Supervisors:
Dr. Erik Garnett, Prof. Dr. Albert Polman (second assessor)

Thesis on research for Bachelors Project
Natuur- en Sterrenkunde (18EC)
February - June 2013

ABSTRACT Nanophotonics has become very important in the development of third generation solar cells, based on high-efficiency thin-film technology. Nanowires may enable this because of their radial geometry and because they support resonances. Recent research suggested that a metal nanowire with an extremely thin semiconductor shell could further improve efficiency; it theoretically predicted an increase in both the absorption per resonance and the number of effective resonances in this coaxial geometry. Also, the metallic core could act as an electrode for a local contact. This project was aimed at verifying this theory, by answering the following research question: What are the resonances in scattering spectra of $Cu@Cu_2O$ core@shell nanowires of different core-shell dimensions, and how does this compare to theory? Therefore $Cu@Cu_2O$ core@shell nanowires were synthesized in aqueous solution at room temperature and the dimensions were analyzed by using transmission electron microscopy (nanowire core diameters 39-124nm, average 67.3nm; shell thicknesses 25-41nm, average 34nm) The scattering spectra were obtained using cathodoluminescence (CL) spectroscopy on seven $Cu@Cu_2O$ nanowires. Two of the seven wires that were measured showed a narrow wavelength peak between 650-660nm, close to theory. These two wires had a relatively large core (diameter: 80nm and 124nm). The other wires showed broad resonance peaks. This difference could be explained by theory: in a relatively large core ($\gg$50nm) scattering exceeds absorption, giving a clear response. In a smaller core scattering gets damped. Although some resonance peaks matched with theory, other peaks that were predicted did not appear experimentally. Scanning electron microscope images showed rough wire-surfaces that probably extinguished photonic modes, leaving only the plasmonic resonances visible. Also, asymmetric line scan profiles indicated carbon deposition on the samples which could have affected responses. Future research will use different equipment to allow for both optical excitation and detection of resonant modes, which can provide additional information about these characteristics. Finding the optimal nanowire material and dimensions could lead to the discovery of ideal building blocks for highly efficient solar cells.

Bachelor Bèta-gamma & Physics
University of Amsterdam
FNWI, The Netherlands

UNIVERSITEIT VAN AMSTERDAM

Center for Nanophotonics
FOM Institute AMOLF
Amsterdam, The Netherlands

FOM Institute AMOLF

Contents

Chapter 1

Introduction

The field of nanophotonics plays a critical role in the development of so-called 'third generation solar-cells' [1]. The fundamental feature of these nanoscale solar cells is that their sizes are similar to or even smaller than the wavelength of light, so that light can be trapped which can dramatically increase their efficiencies compared to other generation solar cells. Research on third generation cells is mainly focused on high-efficiency thin-film technology, with the aim of combining these high-efficiencies with drastically reduced material and fabrication costs, so that these cells can match up in the competition with fossil fuel techniques in becoming a cost-efficient source of energy[1]. Until recently, thin-film solar cells have had limited efficiencies because the absorption of light near the band gap is small or the carrier diffusion length too short[2]. Therefore current research aims to enhance light absorption within thin films by nanostructuring the solar cell for better light confinement. The radial geometry of nanowires has been of great interest because of its benefits in reducing absorption losses and enabling rapid charge separation and efficient carrier collection [3]. Metal nanostructures are beneficial because they support 'localized surface plasmons': oscillations of excited, conduction band electrons in nanoscale materials. By properly engineering the dimensions of a metal nanowire and coating it with a semiconductor shell as the photovoltaic active layer, incident light can couple to either the plasmon modes of the metal core or to the photonic modes of the semiconductor shell, resulting in a resonance that can enhance the probability of photon absorption [4]. Such core@shell nanowires show great promise because they can possibly be mass produced via bottom-up synthesis, both the dimensions of the core and the shell can be tuned to absorb at wavelengths corresponding to the sun's spectrum and semiconductor band-gap, and the metal core can act as a high-performance transparent electrode for local contacts. Overall, this coaxial geometry could be an ideal building block for high-efficiency solar cells.

Just recently, an analytical model that describes light trapping in single metallic nanowires covered with an extreme thin semiconductor layer has been published[4]. This theory demonstrated that it is possible to maximize absorption in a core@shell nanowire, by tuning the sizes of both the metal core and the semiconductor shell to 1) ensure maximal absorption in each resonance mode and 2) increase the total number of degenerate resonances. This theory could be applied to core@shell nanowires composed of different types of metal cores and semiconductor shells[4].

The aim of this research was to experimentally verify this theory. Analytical models were set up beforehand, and have been used as a reference for both the theoretical framework (see Section 2) and the experimental research in this project (see Section 3). The theory has been applied to copper nanowires covered with cuprous oxide as the semiconductor layer. The main research question was: what are the resonances in the scattering spectrum of $Cu@Cu_2O$ core@shell nanowires of different dimensions, and how does this compare to theory?

In this research, $Cu@Cu_2O$ nanowires were synthesized in aqueous solution at room temperature. These single nanowires (nanowire core diameters 39-124nm, average 67.3nm; shell thicknesses 25-41nm, average 34nm) were then measured using cathodoluminescence (CL) spectroscopy. Details on the CL measurements and data analysis can be found in Section 3. The experimental results were then compared to theory, leading to insights into resonances in core@shell nanowires. Discussion on the results and suggestions for further research are introduced in Section 5. Because the science of light interactions with nanowires is an advanced topic, the coming chapter will not only focus on the analytical model, but also give a theoretical framework on how light can be converted into electricity within these types of solar cells.

Chapter 2

Theoretical Framework

The experimental work done for this project was based on theoretical predictions. This chapter will focus on the theory required to understand the basic concepts of nanowires as new types of building blocks for solar cells, on understanding why core@shell nanowires can increase photovoltaic efficiency, and understanding how cathodoluminescence measurements help in confirming this theory experimentally.

2.1 Nanowires for resonance-enhanced photovoltaics

The conversion of light to electricity in a solar cell can be divided into four steps: photon absorption, exciton creation, exciton separation to free carriers and carrier collection by the electrodes [3]. When an incident photon gets absorbed by a semiconductor, it excites an electron from its valence band leaving behind a 'hole': an electron-hole pair (an exciton) is formed. This exciton could then recombine and dissipate heat or release a photon, or this exciton could get dissociated. In a solar cell the latter is strongly desired because to generate power these charge carriers (electrons and holes) must be able to 'travel' through the semiconductor in opposite directions and get collected by the electrodes. The main challenge in photovolotaic research is to create a system that makes optimal use of the incident photons[5].

The use of nanowires as building blocks for solar cells has been recommended, because their nanoscale radial geometry can reduce losses in all conversion steps mentioned above[3]. The first step -reduce losses in photon absorption - is of importance to the theory discussed in this research. An approach to minimize absorption loss, is to to increase the absorption efficiency η_{abs} (the maximum amount of photons that can be absorbed and thus excite electrons) by making sure the photons stay in the system long enough to increase the absorption *possibility*. This can be achieved by creating a *resonance*: the light (energy) gets temporally stored in the system in for example a whispering gallery mode. A second method for increasing absorption has already briefly been mentioned in the Introduction (Section 1): by enclosing a metallic structure in a semiconductor, light can excite localized surface plasmons (LSPs)[1], with high field intensity outside the metal structure, thereby increasing the absorption probability in the semiconductor. The plasmon resonance depends strongly on the intrinsic optical properties and the geometry of the used material(s) [2]. These electron oscillations produce a dipolar field outside the material, which leads to an enhanced absorption and scattering cross section for electromagnetic waves, and also a strongly enhanced electric near field around the metal[6].

2.2 Absorption efficiencies and resonance

Depending on the dimensions and the material of a system, it will interact with a certain amount of power from the incoming energy: σ_{ext}, the extinction cross section. The total extinction consists of scattered and absorbed power: $\sigma_{ext} = \sigma_{sca} + \sigma_{abs}$. A specific maximum amount of energy can be absorbed, related to the maximum absorption efficiency η_{abs}:

$$\eta_{abs} = \frac{\sigma_{abs}}{\sigma_{geo}} \tag{2.1}$$

[1] A surface plasmon is a bound electromagnetic wave at a metal dielectric interface, due to coherent electron oscillations in the metal which decays exponentially perpendicular from the surface[6].

where σ_{abs} is the absorption cross section, and σ_{geo} the geometrical cross section. Note that σ_{abs} can be bigger than σ_{geo} due to the 'antenna effect'. This σ_{abs} is a general definition of what happens when light interacts with a material: it actually describes the amount of power that gets absorbed, related to the amount of power that comes in at the material -or say the effective area that governs the probability of absorption - and is therefore important in describing the optical characteristics of nanowires. Both the η_{sca} and the η_{ext} can be formulated likewise; $\frac{\sigma_{sca}}{\sigma_{geo}}$ and $\frac{\sigma_{ext}}{\sigma_{geo}}$, respectively.

The cross sections σ are highest at specific wavelengths, which correspond to so called resonances, and depend on either the material of the wire or the sizes of the wire. Also different resonances can occur in a wire at different wavelengths. Figure 2.1 shows a graph of scattering efficiencies of two solid semiconductor nanowires of different diameters, plotted against wavelength. Here you can clearly see resonance peaks at a wavelength depending on wire material and diameter.

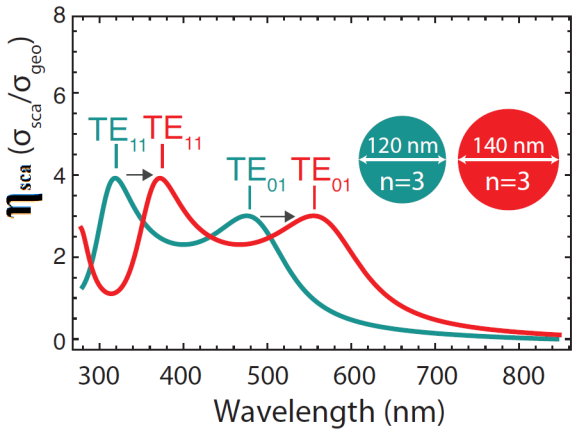

Figure 2.1: Scattering efficiency of a solid nanowire with refractive index n=3 plotted against wavelength. Comparison of two different resonant modes (TE_{11} with TE_{01}) with differences in nanowire diameter (120 and 140nm). Different resonance modes clearly relate to different resonance-wavelengths, and changing the size of the diameter also shifts the scattering profile[4].

Dielectric structures support resonances, based on morphology. These resonances are better to understand from the concept of leaky mode resonances (LMRs)[7]. Leaky modes were once defined as modes with propagating electromagnetic fields outside the structure as opposed to guided modes, which have an exponentially decaying field outside the structure and thus have energy moving away. So LMRs are resonant modes that can couple to incident light, and so to say became leaky because of the small size of the nanowire. This led to interaction with the outside world and in this case the electromagnetic field of incoming (sun)light. For wavelengths close to these leaky modes, the nanowires act as cylindrical cavity that confines this radiation (see Figure 2.2 (a)). This can also be related to the antenna effect, in which a near-field couples to a material and increases the area in which photon absorption is probable [8] [7]. These LMRs that correspond to peaks in scattering and absorption spectra of nanowires will from now on be better defined in terms of TM_{ml} or TE_{ml}. Under normal incidence of light, the polarization of this electric field distribution relative to the wire defines the modes: TE (transverse electric; the electric field is oriented perpendicularly to the nanowire axis) or TM (transverse magnetic; electric field is oriented along the nanowire axis) modes. The m refers to the angular nodes in the field distribution and for example m=2 means that a specific wavelength can roughly resonate around a wire twice. The l corresponds to the number of radial field maxima that exist in a material.

For example: by implementing the dielectric functions of some semiconductor in the analytical model and choosing a radius, the expected scattering for that specific wire in TE polarisation for m=0 and m=1 can be calculated and plotted exactly, to find resonances. Also, by calculating multiple resonances for different modes and polarisations and adding these, the total expected scattering can be plotted. The m=0 mode is angle-independent and thus only occurs once in a wire, whereas the $m \geq 1$ modes can resonate both clockwise as well as counterclockwise. It makes sense to calculate total scattering by adding one m=0 mode with twice the $m \geq 1$ mode. These expected resonances can also be plotted in terms of a electric field intensities (see Figure 2.2 (b,c)).

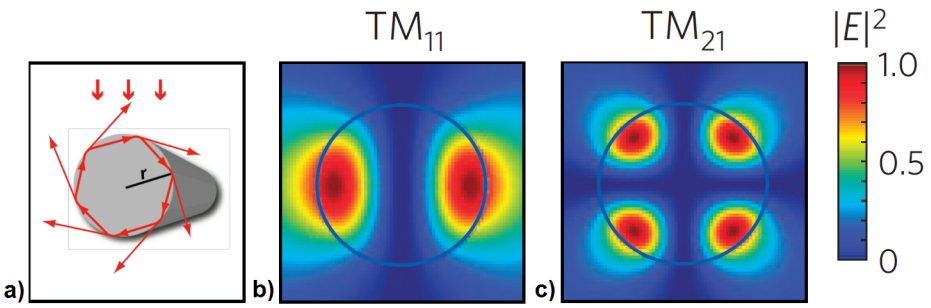

Figure 2.2: **a)** When wavelengths of incident radiation match the leaky modes of the material, a nanowires can act as a cylindrical cavity that confines this radiation inside. Some light can leak out and interact with the surroundings. **b), c)** Two typical examples of different resonances that can occur in a nanowire, in terms of electric field intensity plots (blue circle indicates nanowire/air interface), with the red color corresponding to a high electrical field intensity. These plots correspond to a TM_{11} (b) and a TM_{21} (c) mode[7].

To calculate these scattering and absorption properties of nanowires, one needs the cross section σ. This could be calculated after knowing the electric field distributions of the regions in the wire, which were studied using Mie theory- one of the most prominent theories for analyzing the optical properties of spherical and cylindrical shaped systems. By using the Maxwell equations applied to an infinitely long cylinder, one could calculate modes that correspond to leaky modes: the TE_{ml} and TM_{ml} [7]. Solving the boundary conditions to the Maxwell equations led to a system of equations needed to calculate the Mie coefficients, that could be used to eventually set up an expression for the total amount of absorption in a wire [9][4]:

$$\eta_{abs}^{TE} = \sum_{m=-\infty}^{\infty} \eta_{abs,m}^{TE} = \sum_{m=-\infty}^{\infty} (\eta_{ext,m}^{TE} - \eta_{sca,m}^{TE}) \tag{2.2}$$

These definitions were here defined in TE polarization. These efficiencies are defined as follows:

$$\eta_{sca}^{TE} = \sum_{m=-\infty}^{\infty} \eta_{sca,m}^{TE} = \sum_{m=-\infty}^{\infty} \frac{2}{n_0 k_0 r_{out}} |a_m|^2 \tag{2.3}$$

$$\eta_{ext}^{TE} = \sum_{m=-\infty}^{\infty} \eta_{ext,m}^{TE} = \sum_{m=-\infty}^{\infty} \frac{2}{n_0 k_0 r_{out}} Re(a_m)^2 \tag{2.4}$$

With n_0 the refractive index of the medium (in this case the nanowire), k_0 the free space wavenumber, r_{out} the outer radius of the wire, m the angular mode of the wave equation and a_m the Mie coefficient[4]. The calculations show that the resonances can be calculated per fixed radius of the cylinder, which led to the conclusion that changing the diameter of the wire affects the resonant wavelength [8].

The absorption cross section σ_{abs} is defined ad follows[4]:

$$\sigma_{abs} = \frac{2\lambda}{\pi} \frac{\gamma_e \gamma_i}{(\omega - \omega_0)^2 + (\gamma_e + \gamma_i)^2} \tag{2.5}$$

This σ_{abs} changes at different diameter/wavelength combinations, which define a wavelength where there is resonance. The maximum amount of absorption is limited by the value $\lambda\backslash 2\pi$. This value is reached when *critical coupling* arises; the radiative loss rate γ_e equals the absorption loss rate γ_i of the resonator (γ_e=γ_i), at resonance frequency (ω=ω_0) and the following formula is satisfied[4]

$$\sigma_{abs,max} = \frac{\lambda}{2\pi} \tag{2.6}$$

The above information was needed to understand how nanowires can act as a resonance-enhanced photovoltaic. Now it is time to turn to the theoretical predictions on core@shell nanowires. Next section will show that using a metal core in the radial geometry not only supports whispering gallery modes, but that a semiconductor shell also introduces Fabry-Pèrot resonances.

2.3 Analytical Predictions Core-Shell Nanowires

The previous section discussed some requirements on how to increase absorption in a nanowire. Resonances are the key principles in achieving this, and by ensuring these are critically coupled one can even maximize absorption of each individual resonance. By wrapping a semiconductor layer around a metal nanowire and creating a core@shell nanowire, even higher efficiency can be achieved. The analytical model that supports this theory showed how to increase the total number of degenerate resonances. In contrast to theoretical studies that have been done before, this model focused on how the wires' thicknesses determined the interaction with incoming light [7][10]. This gave new insight about additional resonances that came from the specific configuration, which lead to a proposition for more efficient absorption by using extremely thin semiconductor shells. Written below will follow a recapitulation of this theory, with supporting information needed to understand the aspects of the measurements done on the wires[4].

Previous research on core@shell nanowires showed that wrapping a semiconductor layer around a cylindrical shape would perturb polarization-dependent Mie modes which would transform to polarization-independent Fabry-Pèrot (FP) like resonances. The condition that then must be satisfied is

$$a > \frac{b}{n} \tag{2.7}$$

where a is the inner diameter of the core, b is the outer radius, and n is the refractive index of the shell [11]. By extending the Mie theory for cylinders to core-shell nanowires, and taking into account condition (2.7), this addition of FP resonances made it possible for distinct LMRs to add up linearly, and cause the absorption peak to be higher (see Figure 2.3)[4].

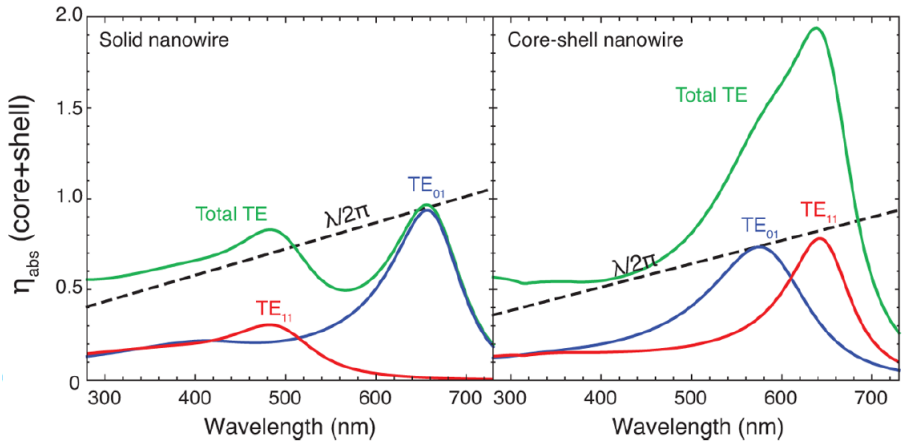

Figure 2.3: Comparison between a solid a-Si nanowire of a 110nm (left) and a 88nm silver core diameter with a 18nm a-Si shell (right); in the latter adding up resonances achieved higher efficiency [4]

.

Under normal incidence, FP resonances are insensitive to polarization. So this core@shell geometry introduces more resonances in both polarizations (see Figure 2.4).

Overall, this model shows that there is a strong relation between core and shell thickness and the resonance peaks in the wires. For every material a different optimal core and shell thickness exists, which can be found after implementing the dielectric constants of the used material [12]. These different optimal dimensions of a material are due to the differences in band gap energy and refractive index, but for all a relatively bigger core would be of most interest because in this case the transformation to

FP resonances occurs. The combination of those specific dimensions led to the paradoxical conclusion that for most resonances the absorption in the semiconductor increased when the absorption coefficient decreased; when it is critically coupled. Also extreme absorption could be demonstrated by increasing the total number of degenerate resonances. This maximization of absorption in a structure that is less polarization dependent is showed to be an ideal building block for solar cells[4].

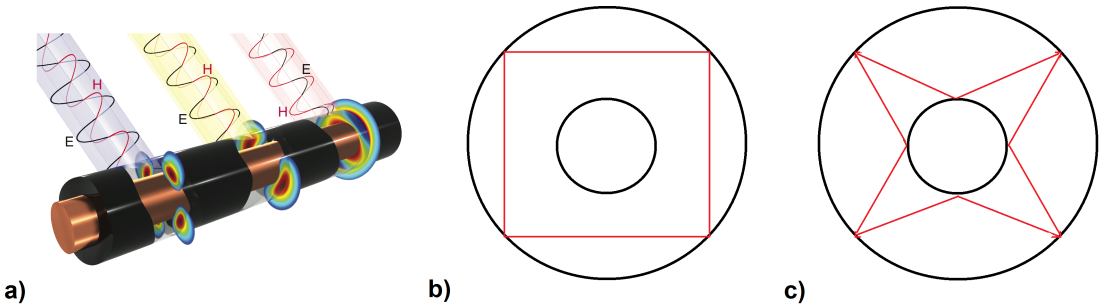

Figure 2.4: **a)** Schematic representation of different orientations of the incoming electromagnetic field with different wavelengths, resulting in resonances that can occur in the core-shell nanowire[4] **b)** Schematic representation of Mie-like modes compared to **c)** Fabry-Pèrot-like resonance modes.

Chapter 3

Methods and Experimental Setup

In this Section the development of a method to synthesize shells around metal nanowires will be discussed. Because the concept of synthesizing shells around metal nanowires in solution is quite new, it has so far not been possible to exactly tune the dimensions of the core-shell wires. Therefore before performing CL-spectroscopy, the dimensions of the synthesized wires were first analyzed using transmission electron microscopy (TEM). In the next subdivisions these steps will be discussed in further detail, followed by the actual method of measuring optical responses with CL.

3.1 Sample Preparation

3.1.1 Cu@Cu_2O Core@Shell Nanowire Synthesis

The shell synthesis was partially based on a synthesis done on silver nanoparticles [13]. By adding reagents to copper nanowires (CuNW) in aqueous solution at room temperature, the surface of the wires would react and thus chemically grow a Cu_2O shell around the wire. The hypothesis was that different amounts of chemical precursor injections would result in different thicknesses of Cu_2O shells.

Four samples were made, with different amounts of components, labeled sample C1, C2, C3 and C4. The CuNW in stock (1mg/ml) came from NanoForge, the other components from Sigma-Aldrich. For all four samples, the next procedure was followed:

- Put 8.5 mL of DI water in a vial
- add 300 μL of CuNW in stock
- add 66 μL of 0.1M sodium citrate
- add 160μL of 20mM $CuSO_4$, then shake
- add 660 μL of 0.1M ascorbic acid
- add 90 μL of 1.0M NaOH, immediately shake
- put away for at least 30 minutes to have a reaction occur

Which led to a chemical reaction;

$$2Cu^{2+} + 2OH^- + C_6H_8O_6 \Rightarrow Cu_2O + H_2O + C_6H_6O_6 \tag{3.1}$$

With $C_6H_8O_6$ ascorbic acid and $C_6H_6O_6$ dehydroascorbic acid. The other components acted as coordinating ligands.

All the samples were bright and salmon colored; probably affected by addition of the copper-colored CuNW in DI water. After 30 minutes, in samples C2, C3 and C4 extra injections were added, as follows:

- add 66 μL of 0.1M sodium citrate
- add 160μL of 20mM $CuSO_4$, then shake

- add 660 μL of 0.1M ascorbic acid
- add 90 μL of 1.0M NaOH, immediately shake
- put away for at least 30 minutes to have a reaction occur

Sample C1 was now darker compared to the other three samples. After 30 minutes, samples C3 and C4 got an extra injection, same as before. Vials were shaken, then put away for 30 minutes. Samples C3 and C4 were clearly more orange than C1 and C2. C1 was still darkest (see Figure 3.1). After 30 minutes only C4 would get an extra injection as mentioned before, and after 30 minutes this sample was the lightest of four. These differences in color can be explained by the extra injections which made the samples more diluted. Also these extra injections could have resulted in the formation of nanoparticles, which have different properties in light absorption/scattering than nanowires.

45 minutes after the last injection, all four samples were cleaned; the precipitates were separated from the solution by centrifuging at 2000 rpm for 6 minutes and then 3000 rpm for 4 min. After cleaning with ethanol, the samples were centrifuged again at 3000 rpm for 4 min. They were then redispersed with ethanol and dropcasted on TEM grids [1].

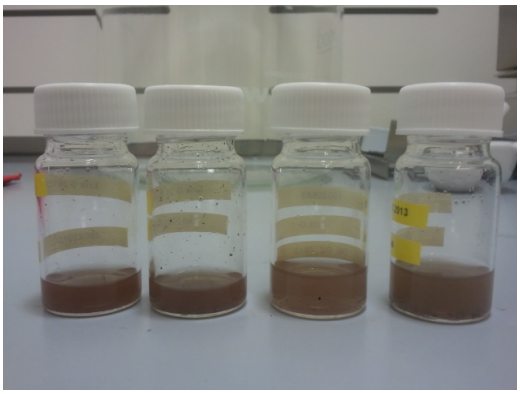

Figure 3.1: Cu@Cu_2O nanowires in solution; named Cx, with 'x' standing for number of injection of Cu_2SO_4 added to the copper nanowire solution. Four samples after cleaning, from left to right C1, C2, C3, C4.

3.1.2 Transmission Electron Microscopy

To obtain the dimensions of the cores and the shells of the synthesized wires, respectively, transmission electron microscopy (TEM) was performed. TEM made it possible to 'look' through the sample to check whether the shell-synthesis actually worked, and to make images of specific wires to acquire the core-shell dimensions. This TEM was done at the University of Utrecht with a Tecnai 20 FEG [2].

TEM is a microscopy technique that is used to study small details of materials down to near atomic levels. With TEM, a beam of electrons gets transmitted through a sample and detected on a substrate. This forms an 'image' on the substrate which then gets focused at a detector that is able to magnify the image. A modern TEM is composed of an illumination system as the source of the beam, a specimen stage, an objective lens system, a magnification system, data recording systems, and an analysis system. The TEM used in this project was equipped with a Schottky field emitter, capable of and unique for performing high coherence lattice imaging, electron holography, and high spatial resolution microanalysis[14]. This TEM was also capable of focusing the electron beam into a narrow spot which was scanned over the sample for mapping samples (also called scanning tranmission electron microscopy (STEM)). By using an annular dark-field detector for this mapping -a method of collecting electrons from an annulus around the beam - an image got formed only by the most high angle scattered electrons: high-angle annular dark-field imaging (HAADF). This is also called Z-contrast imaging because of the enhanced scattering from high atomic number atoms. It gives even more precise images of the nanowires.

All four samples C1, C2, C3 and C4 were analyzed with TEM, and per sample an appropriate grid was chosen and the wires on this grid were then labelled 'wire1', 'wire2', 'wire3', ... (see Figure 3.2).

[1] 01800N-F Formvar/Carbon 200 mesh, Nickel, approximate grid hole size: 97μm. Ted Pella inc.©
[2] See EMU: Electron Microscopy Utrecht. *http://www.electronmicroscopy.nl/facility/facility.html*

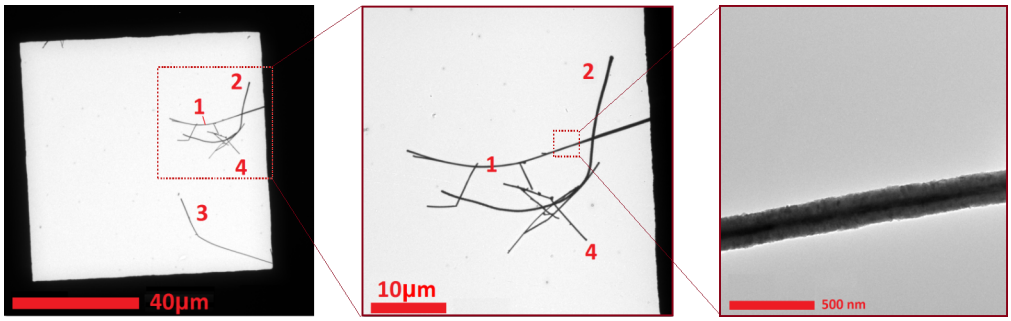

Figure 3.2: Three images of sample C3_grid1, zoomed in until you can clearly see a shell around nanowire 1. Red numbers and lines are added to clarify the position of the mentioned wires, and position of zooming.

3.1.3 Image Analysis

The TEM, STEM and HAADF images acquired were equipped with a scale-bar. All these images were then analyzed to obtain the actual seizes of the core diameter and total diameter of each wire. In some cases, multiple images were taken from the same wire at different spots, so analyzing different images would obtain a possible error in this Image Analysis (see Figure 3.2, third image for TEM).

3.2 CL-measurements

Cathodoluminiscence (CL) spectroscopy is a method capable of measuring optical responses in dielectric photonic crystals and nanostructured photonic materials with nanometer-scale resolution. The term 'cathodoluminescence' refers to photonic emission (luminescence) as a result of electron beam irradiation (cathode-ray = electron beam). The basic concept of CL-measurements originates from the coupling of a high-energy electron's electric field to the local modes of a photonic structure, which leads to emission that can be detected[15]. This emission is directly linked to the local density of optical states (LDOS) of the material at which the e-beam is aimed. By scanning a tightly focused electron beam over the surface of a sample, the incident electron and it's image charge together form a dipole, which couples to the modes of the structure, giving an insight in the available resonances [16] [15]. By collecting the generated emitted light spectrum at every beam position, a 2D map of the photonic material's LDOS was made, which gave an insight in the resonances of the nanowires.

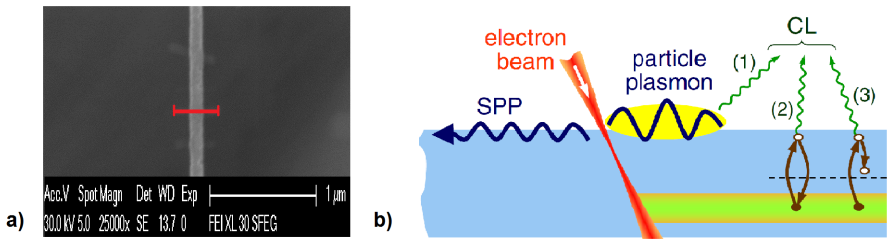

Figure 3.3: **a)** Image of the line scan done on a core-shell nanowire. The red line indicates the length and direction of the electron beam over the nanowire. This could either be from left to right or right to left. **b)** Schematic representation of excitation processes triggered in a sample by an electron beam. The beam can launch propagating SPPs or produce LSPs in particles which could couple to radiation (1). Electronic excitations or excitons in the sample can decay back to the initial state [coherent CL emission (2)] or to a different excited state [incoherent CL emission (3)][16].

The CL measurements were performed using a field emission scanning electron microscope extended with a modified Gatan ParaCL cathodoluminescence system (see Figure 3.4).The electron beam operated

at 5, 20 and 30 keV, respectively, depending on the particular measurement. It's spot-size had a diameter of several nanometers. At first, the setup without lens and flip mirror and with a CCD camera was used to align the the electron beam with the focal point of the mirror to have it focused on the sample. The sample (TEM grid) was placed on a stage at a working distance of about 13.6(2) mm between pole piece and the sample, and at a distance of about 0.5 mm between the mirror and it's focal point. After aligning the setup, the lens and the flip mirror were put back in position to collect counts (CL-intensity) in the spectrometer. The spectral resolution was about 5nm, the grating used 650 nm which means that the system is sensitive for the wavelengths 360-940 with a resolution of the spectrometer of 1.7 nm, and adjusted to the numerical aperture of the fiber, which is about 5 nm total spectral resolution. The data will then get collected with an integration time of 1, 2 or 4 seconds, respectively, depending on the measurement.

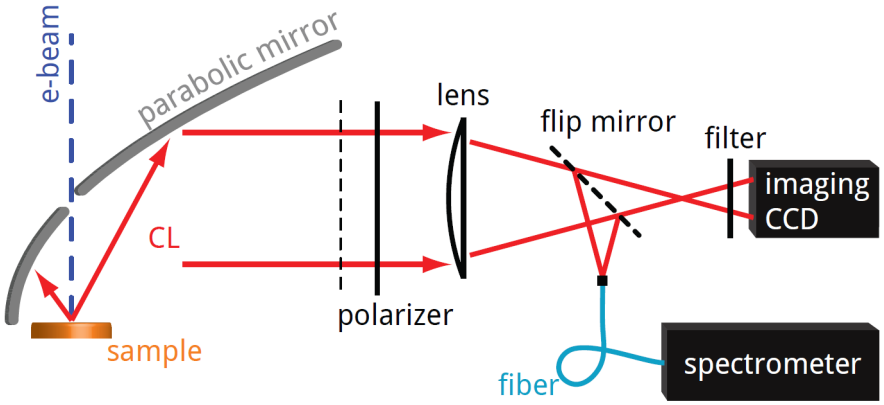

Figure 3.4: Schematic display of the CL setup (not to scale). An electron beam on a sample causes photonic emission that is collected by a parabolic mirror. The CCD camera can be used to directly monitor the alignment of the mirror or to measure the angular emission patterns. Alternately, a flip mirror can be used to guide the light into a spectrometer and measure the intensity of the emission spectrum[15].

Only the spectrometer was used in the CL measurements. CCD is mostly used for angle-resolved measurements. Before every measurement, a drift correction was executed, which made sure the position of the e-beam couldn't change relatively to the wire while scanning. The electron beam would move along a straight line perpendicular to the length of the wire, as can be seen in Figure 3.3 a).

3.3 Data Analysis

The data was analyzed using a Matlab code pre-written at the AMOLF institute[3]. This code corrects the raw data taking into account calibrations and system losses of the specific parts of the used setup, based on their system responses. For example: the detector is less sensitive for certain wavelengths in the blue because of certain losses in both the mirrors and lens of the system and because of the sensitivity of the grating of the spectrograph. Also, by averaging over multiple background spectra, it minimizes noise. Both references for dark data and references on the substrate were performed. Averaging over pixels, the use of conversion lists (grating position, grating) and normalization of the whole response to 1 eventually gave a data-set that could be used to plot the results in terms of wavelengths. This gave a SEM Line Scan which shows the SE (secondary electron) intensity plotted against the scan position in nm. Another graph showed the CL Intensity (in arbitrary units-because of the corrections) of the response plotted against the wavelength.

[3]FOM-Institute for Atomic and Molecular Physics (AMOLF). Amsterdam, The Netherlands

Chapter 4

Theoretical and Experimental Results

An over- and review of the most relevant results of both the experimental work and the theoretical predictions will be outlined in this section. These results are then compared and discussed in some detail. The next section will discuss the project as a whole, by focusing on the most interesting outcomes.

4.1 Wire Analysis

After the image analysis, the following dimensions of the core@shell nanowires were found in the four different samples: C1 contained nanowires with dimensions ranging from core diameters of 39-124nm (average: 67.3nm) and shell-thicknesses ranging from 29-41nm (average 34nm). C2 wires had core diameters of 41-160nm (average 76.8nm) and shells 19-48nm (average 34.4). C3: core diameter 28-161nm (average 70.4nm), shells 51-79nm (average 66.6nm). C4: core diameter 39-80nm (average 60.8), shells 35-79nm (average 58.4nm). More nanoparticles were found in the samples with extra chemical precursor injections. It seemed that these extra injections led to thicker cores, though no obvious conclusion could be drawn. Up to six wires per sample were analyzed, so if there was a difference in dimensions because of the various reactions, this analysis couldn't state this. Therefore there was no preference which of the four samples was used for CL-measurements.

Sample C1_grid1 had been analyzed. The measurements were done on wires 1 to 6 (see Figure 4.1), which had the dimensions showed in Table 4.1. (Another measurement was done on a random wire, which was called wire 7.) Figure 4.1 shows an image with an overview and position of the nanowires.

Sample name	**⌀core (nm)**	**error(nm)**	**shell thickness (nm)**	**error(nm)**
C1-grid1-wire1	39	2	34	3
C1-grid1-wire2-STEM1-HAADF	68	1	29	1
C1-grid1-wire3-STEM1-HAADF	80	1	38	1
C1-grid1-wire4-STEM1-HAADF	39	1	29	3
C1-grid1-wire5-STEM1-HAADF	54	2	41	1
C1-grid1-wire6-STEM1-HAADF	124	2	33	2

Table 4.1: List of thicknesses of nanowires 1 to 6 in sample C1_grid1. The error was based on the inaccuracy of the image analysis and the difference in shell thickness left and right of the core. The sample name indicates whether a STEM and or HAADF imaging was performed.

After analyzing the CL-data in Matlab and comparing the outcomes per electron beam-voltage and integration time, two significant connections between measurements were discovered. These will be further explained in the next subsections, and compared to theory. The resonant peaks that could be calculated with the theory don't change significantly by altering a couple of nanometers of the core diameter and the shell thickness, respectively. Therefore the error listed in Table 4.1 was not taken into account in the calculation of the theoretical predictions and in the comparison with the experimental results.

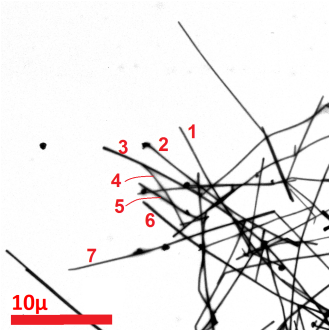

Figure 4.1: Image of C1_grid1, with the labeled nanowires indicated by red numbers.

4.2 Resonances found

The CL-data produced two graphs; one was a 'SEM line scan' divided in five sections by five colored lines (see Figure 4.2 and 4.3). The red line indicates the number of counts at the point where the electron beam starts to scan over the edge of the wire. Note that at this point, the electron beam is incident at only the shell of the wire. The brown line indicates the point where core starts to get into account. The green line matches the point right above the center of the wire, the grey line conforms the brown one but then on the other side of the wire, as well as the blue line which conforms with the red line. The second graph, the 'CL counts Line Scan', shows which wavelength corresponds to a higher intensity number of detected CL. The number of counts in the CL counts Line Scan is in arbitrary units, as these counts have been subject to a lot of corrections in the Matlab code.

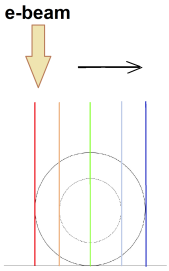

Figure 4.2: Schematic figure of the line scan performed by the electron beam during CL-measurements, with the different positions on the wire indicated by different colors. These colored lines match the colors in the collected line scan images.

The theoretical scattering spectra predicted multiple resonances. Hence wire 3 and 6 jumped out, as their experimental data too showed narrow peaks at a well defined wavelength, as seen in Figure 4.3. Both wire 3 and wire 6 show a clear peak at 660nm and 650nm, respectively (see Figure 4.3), whereas wire 3 seems to also show a peak at 890nm, and wire 6 at 940nm. For wire 3, the first peak seems to be strongest at the point where the core gets hit by the electron beam (brown curve) and for wire 6 both the intersection of core-shell and the middle point of the wire showed brought forth the most counts. This could be explained by the core and shell thickness which differs for the two wires.

By comparing the latter to wire 4 for example, one sees a difference between the shape of the peaks (see Figure 4.4); in the CL graphs of wire 4 no narrow peak can be found. There is a 'bump' between 650-850nm that could indicate a resonance, but the peak is very broad compared to those in data of wire 3 and wire 6. The peak is thus less convincing, and redshifted compared to theory (see Figure 4.5). The same arguments can be applied to the outcomes of wire 2. Wire 1 and wire 5 (see Figures 4.4 and 4.6) show a very broad spectrum with some small peaks. These peaks are not very intense and thus less convincing also.

An evident correspondence between wires 3 and 6 is that these two have a relatively larger core compared to the other wires. Also, Figure 4.6 shows the theoretical predictions of wires 3, 5 and 6. The TE1 mode (red curve) has significant influence on the position of the total resonance peak. The resonances predicted by the TE0 (blue curve) could not directly be observed in the CL graphs, but the

high peak seems to agree with the CL outcome. In the predictions on wire 5, the TE0 mode dominates the intensity resonance peak. One assumption is that this TE0 mode is redshifted, which could explain the vague bump between 800-950nm for all wires.

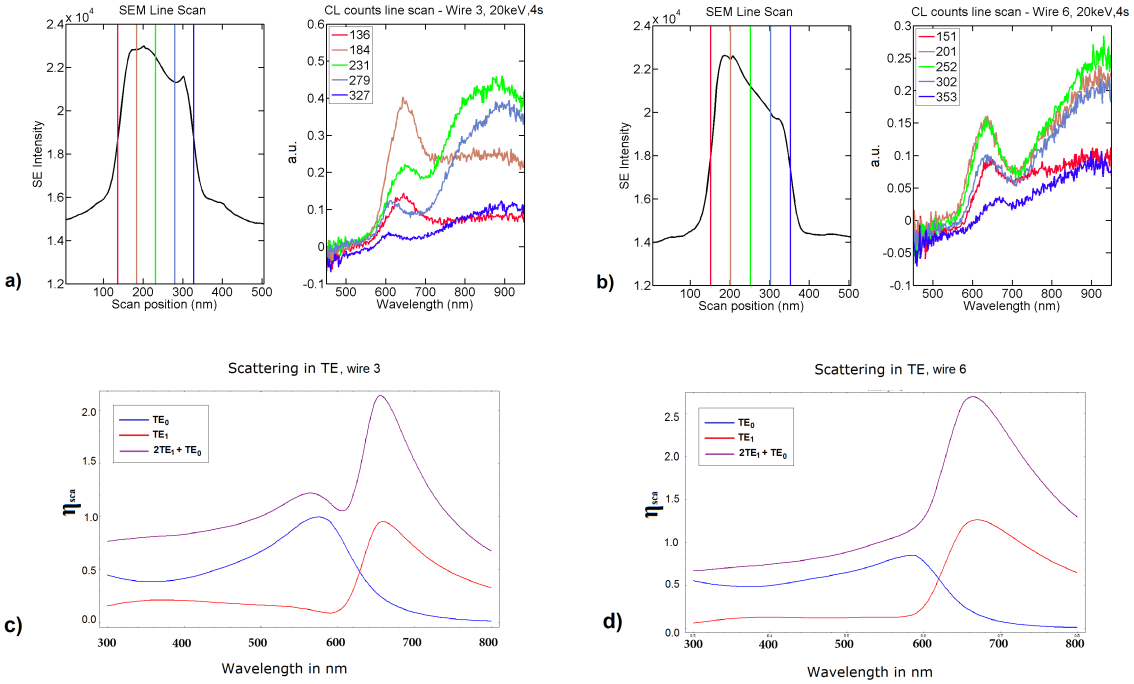

Figure 4.3: Comparison of two CL scans at 20keV, 4 seconds integration time. The SEM line scan shows the scan position divided in five sections, indicated by coloured lines. The CL counts line scan shows the number of relative counts at specific wavelengths. **a)** Wire 3 (core diameter 80nm, shell 38nm), showing a narrow resonance peak at a wavelength of 660nm. **b)** Wire 6 (core diameter 124nm, shell 33nm), showing a narrow resonance peak at a wavelength of 650nm. **c)** Scattering efficiency profile of wire 3 (core diameter 80nm, shell 38nm), calculated by theory. This predicts resonant peaks at 590nm and 680nm. **d)** Scattering efficiency profile of wire 6 (core diameter 124nm, shell 33nm), calculated by theory. This predicts resonant peaks at 600nm and 660nm.

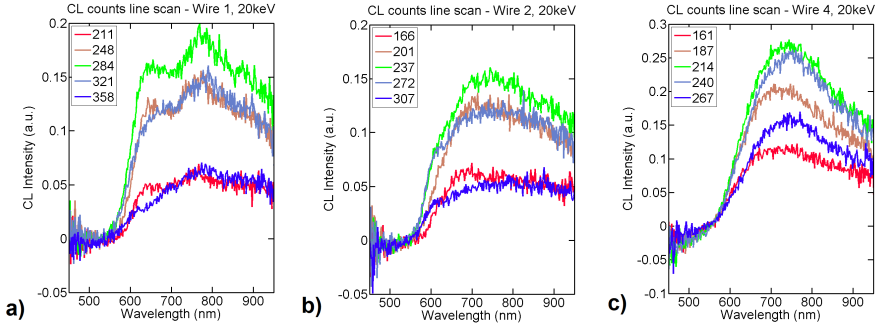

Figure 4.4: CL data on wires 1, 2 and 4, all taken at 20 keV 2 seconds integration time. These CL intensities show bumps that can account for resonances, but are not as convincing as other data. **a)** Wire 1 (core diameter 39nm, shell 34nm), showing two peaks that are not intense at 650nm and 780nm. **b)** Wire 2 (core diameter 68nm, shell 29nm), showing a very broad peak between 600-850nm. **c)** Wire 4 (core diameter 39nm, shell 29nm), showing a broad peak between 650-850nm.

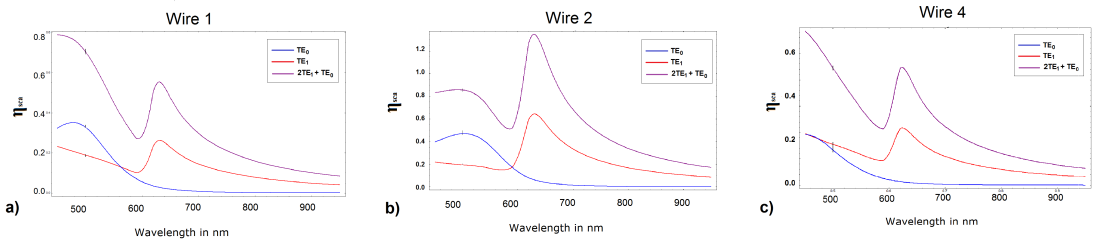

Figure 4.5: Theoretical predictions on wires 1, 2 and 4. The y-axis shows scattering efficiency, the x-axis wavelength in nm from 450 up to 950nm.

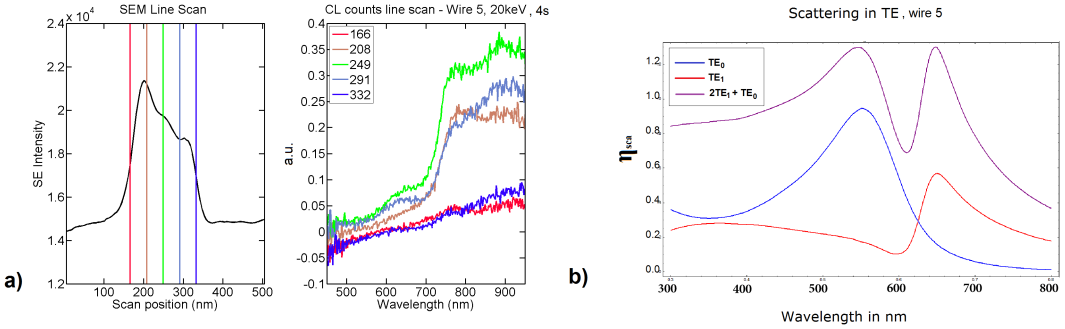

Figure 4.6: **a)** Wire 5 (core diameter 54nm, shell 41nm), CL at 20keV with an integration time of 4 seconds. No well defined peaks can be found in the CL counts line scan. At 880nm a higher CL Intensity is seen. **b)** Scattering efficiency profile of wire 5, calculated by theory. This predicts resonance peaks at 570nm (blue curve) and 670nm (red curve).

4.3 Asymmetric SEM Line Scan

For some wires the profile of the SEM line scan was asymmetric (see Figure 4.7). In most cases the left side of the scan showed a bigger peak than the right, and the 4 seconds integration time showed a bigger asymmetry than 2 seconds. To see whether this was an effect of the direction of scanning over the wire, a random wire (wire 7) was chosen and scanned from both left to right as right to left to see the effect (see Figure 4.8). Both scans on wire 7 showed an asymmetric profile with peaks at the same side -this time on the right side instead of the left - so the scanning direction was probably not the cause of this asymmetry. The position of the asymmetric peak coming from the intensity of secondary detected electrons, could maybe be explained by the position of the wire relative to the detector, or by the structure of the wire (which was not perfectly symmetric). Another explanation could be deposit on the sample, which could explain why the 4s integration time gives a higher peak than the 2s: the longer the scan, the more waste gets burned which deposits on the sample.

The CL data clearly showed narrow resonance peaks for two of the seven wires that were scanned; wire 3 and wire 6. These resonance peaks were at wavelengths that seemed to agree with theoretical predictions. For the wires 1,2,4 and 5 only wide peaks were found in the regions between 700-950nm, which is redshifted in comparison to what theory predicts. All scans showed an asymmetric line profile, that could be explained by deposit on the sample.

The next section will continue in discussion on the results, as will suggest improvements for further research.

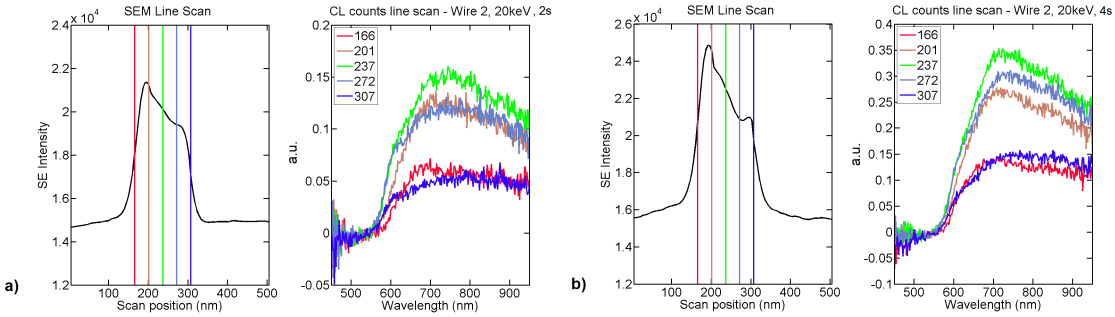

Figure 4.7: SE Intensity and CL Intensity of wire 2 (core diameter 68nm, shell 29nm) at 20keV and an integration time of **(a)** 2 seconds with an asymmetric line scan profile and **(b)** 4 seconds with an even more asymmetric line scan profile. Both a) and b) show no clear resonant peaks; only a bump at 750nm.

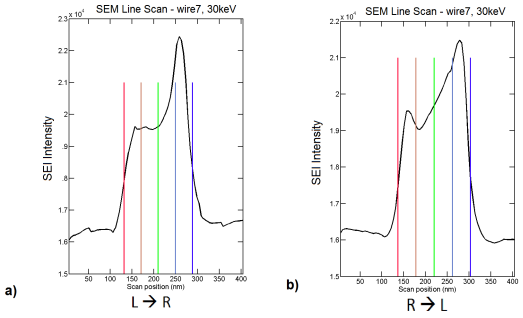

Figure 4.8: Comparison of SEM Line Scan of wire7 (dimensions unknown) from Left to Right (a) and Right to Left (b). Both show an asymmetric profile with a peak at the right.

Chapter 5

Discussion and Suggestions for Future Research

In the experimental results did not exactly match theoretical predictions; no multiple resonances have been found to verify theory, and the resonances that did occur were barely visible except for two wires. These wires 3 and 6 both showed one narrow peak at a wavelength that was predicted in theory. These resonance peaks seemed to match the TE1 mode in the calculated scattering profile. The other 'bumps' that seemed to show, were very broad and less convincing.

From theory the TE0 mode (blue curves in the theoretical prediction plots, Section 4) describes photonic modes, whereas TE1(red curves) describes hybrid plasmonic modes. Because the calculations were based on Mie theory applied to an (infinitely long) perfectly homogeneous cylinder, differences between theory and experiments exist. The synthesized wires had a rough surface (see Figure 5.2), which could result in differences between theory and experiments, assuming that this unequal shell causes more scattering of photonic modes that results in a high radiative loss rate γ_e, respectively (while γ_i stays the same - see Formula 2.2). The rougher the shell, the higher γ_e and the broader (or more unclear) the corresponding resonant peak. Note that the surface of the shell can only influence photonic modes; plasmonic modes are tightly bound to the metal-semiconductor interface and thus not 'see' the rough surface. Assuming that the photonic modes are strongly damped because of the rough surface, one could expect that there is almost zero interaction between resonances (or hybridization between LSPs and photonic modes), which was predicted in theory. So ignoring the photonic modes and focusing on the plasmonic modes, one could refer to classical plasmonic theory to check whether the resonant peaks found in the experiments match the predicted plasmon resonances. Classical theory also relates redshifting of a plasmon resonance to the medium around a metal. In the case of core-shell nanowires, a high-index shell was wrapped around a metal, which according to classical theory results in redshift of resonances, according to:

$$Re(\epsilon_m(\lambda)) = -\epsilon_{env} \tag{5.1}$$

With ϵ the dielectric function of either the medium (m) or the environment/shell (env)[17].

Even though not all results exactly match theory, for two wires a well defined and reasonably explicable resonant peak was found that actually agreed with what was predicted. Both wire 3 and wire 6 have a relatively large core which could explain why only these two wires give rise to clear peaks[4]. A relatively large core (diameter $\gg$50nm) supports more scattering, which actually means a higher intensity of plasmon radiation and relatively less absorption. The bigger the core, the more scattering exceeds absorption (see Figure 5.1).

This doesn't mean that no resonances were present in wires 1,2,4 and 5, but that CL wasn't able to show these modes. The bumps found in wires 1,2,4 and 5 were broader, which can be explained by the absorption that exceeds scattering for smaller cores. This absorption could have damped the detected CL, resulting in a broad resonance peak, and also the lower intensity of the response.

The theoretical calculations could have been performed by using the general theory on core@shell nanowires, and implementing the Palik dielectric constants[4]. It would be interesting to use other materials than Cu and Cu_2O to see whether those predictions match theory, and to see whether other materials are better in supporting resonances. Wires used in further research could be synthesized

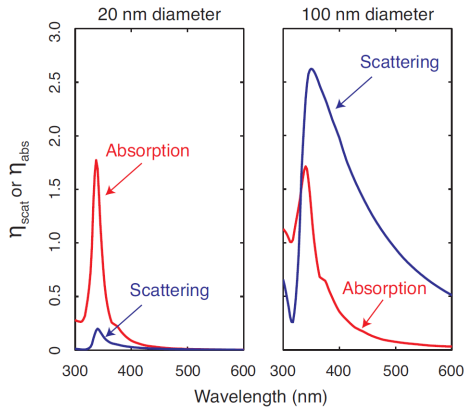

Figure 5.1: Comparison of the η_{scat} and η_{abs} of two silver nanowires with 20 nm diameter (left) and 100nm diameter (right). It shows that the nanowire diameter strongly affects the resonances (scattering or absorption), but does not strongly affect the resonance wavelength[4].

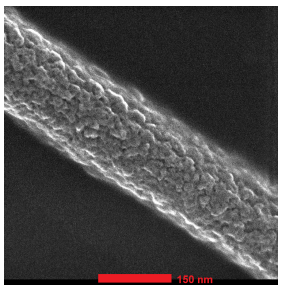

Figure 5.2: STEM image of C1_grid1_wire3, showing the rough surface of the nanowire shell.

differently. The use of other components in solution could maybe create smoother surfaces. Also vertically growing nanowires gives more control over their dimensions[1].

The fact that both the line scan from left to right and the line scan from right to left showed an asymmetric profile at opposite directions, can possibly be explained by the fact that scanning an e-beam over the surface could leave some deposit, which influences the eventual outcome of the scan. Also the bigger asymmetry in the line scan at higher integration time supports this assumption. The fact that the symmetric peak was at different position for different wires (sometimes left, sometimes right), could be explained by the position of the mirror relative to the wire. An attempt has been made to clean the wires using plasma etcher, but this damaged the sample. Despite difficulties with the plasma cleaning, future studies must find a method to minimize surface contamination.

Also, there seemed to be some noise in the region <550nm of the CL-data. This could have a relation with the bandgap of the Cu_2O, which is at 2.137eV ($\rightarrow$580nm). Electrons with energy below this band gap cannot excite states, which could explain why the data below this wavelength is unclear. Another explanation comes from the γ: a higher γ_e could correlate with not finding any resonances, because then the absorption exceeds the scattering. If this was the case, it could explain why no peaks could be detected in a certain wavelength-region.

Future research has some challenges to overcome. Since the electron beam in a CL-setup aims perpendicular to the cross-section of the wire, only TE polarization is directly excited. Experiments that take both light-polarization into account could be very helpful to verify theory, because this includes verification of the TM polarization. But this requires a different setup. Suggested is to use a laser setup, because this could be equipped with a polariser. Also a laser would be able to directly aim a high intensity light-bundle at a tunable wavelength on individual wires by using a strong lens to focus. This could precisely analyze the different resonances that occur in each wavelength-scale at each point of the wire.

Also, predictions on angle dependency have been done to see whether this affects the resonances[7]. It would be very interesting for future research to take this into account.

These suggestions could lead to synthesizing new nanowires existing of efficient materials and smooth

surfaces, that can experimentally be tested on multiple optical characteristics. This will lead to nanowires that efficiently convert (even less intense-)light to electricity, at a large range of wavelengths coming from different angles at different polarizations. Other research is in progress on finding ways to connect nanowires mutually to eventually form a nanowire-network. This network can then be deposited on a thin film and be a new concept of building solar cells bottom-up.

Chapter 6

Conclusions

The main goal in this project was to experimentally find multiple resonances in core@shell nanowires and compare these to theory. Therefore, core@shell nanowires were synthesized and optical measurements were done using cathodoluminescence spectroscopy. With this, the research question "what are the resonances in the scattering spectra of $Cu@Cu_2O$ core@shell nanowires of different dimensions?" could be answered and the results could be compared to theory. Unfortunately, no multiple resonances have been found to verify theory, probably because of the rough surfaces of the shells.

An important result did come out of the measurements: the core@shell nanowires with a relatively large core (i.e. 80nm and 126nm), showed narrow and thus convincing resonance peaks in the CL data, while wires with relatively small cores did not. The CL-data of these two nanowires (wire 3 and wire 6) seemed reliable enough to say that they supported resonances at 660nm and 650nm, respectively.

Although the results did not match theory exactly (predicted resonances were at 670nm and 660nm), these peaks indicate that this is mostly due to the rough shell which could have redshifted the response. The plasmon resonance still shows up, as if should -even in rough inhomogeneous media.

To find multiple resonances in future research, wires with smoother surfaces need to be synthesized, and the samples need to be cleaned before doing measurements. The latter probably explained the asymmetric line scan profile. This can all be avoided by improving the experimental conditions, taking into account the suggestions discussed in the previous Section. Additionally, with a different setup such as a laser, the response to plane wave illumination can be probed, leading to more significant verification of the predicted theory. Such a setup could also expand the research opportunities because of its ability to examine more characteristics of nanowires.

This project has been able to synthesize $Cu@Cu_2O$ core@shell nanowires and use them to do optical measurements on. Although measurements and theory did not agree very well, the mismatch can be explained and the outlook is very promising. The core@shell nanowires do support resonances, probably resulting in a large σ_{abs} with unpolarized response. Also, the metal core can act as a promising candidate for a local contact. The proposed concept of building a cell bottom-up by connecting many nanowires together and depositing this nanowire-network on a thin film would be the basis of a material efficient, thin and light, flexible solar cell. Present research is getting closer and closer in finding this alternative, efficient source of energy, which will contribute in abundant clean energy.

Bibliography

[1] K. Catchpole, S. Mokkapati, F. Beck, W. E-C., A. McKinley, A. Basch, and J. Lee, *Plasmonics and nanophotonics for photovoltaics*, MRS Bulletin **36**, 461 (2011).

[2] H. Atwater and A. Polman, *Plasmonics for improved photovoltaic devices*, Nature Materials **9**, 205 (2010).

[3] E. Garnett, M. Brongersma, Y. Cui, and M. McGehee, *Nanowire Solar Cells*, Annual Review Material Research **41**, 269 (2011).

[4] S. Mann and E. Garnett, *Extreme light absorption in thin semiconductor films wrapped around metal nanowires*, Nano Letters (2013).

[5] J. Twidell and T. Weir, *Renewable Energy Sources*, Taylor and Francis, 2006.

[6] J. van Wijngaarden, *Cathodoluminescence Imaging Spectroscopy on Plasmonic Structures*, Master's thesis, University Utrecht, 2005.

[7] L. Cao, J. White, J.-S. Park, J. Schuller, B. Clemens, and M. Brongersma, *Engineering light absorption in semiconductor nanowire devices*, Nature Materials **8**, 643 (2009).

[8] Y. Yu and L. Cao, *Coupled leaky mode theory for light absorption in 2D, 1D and 0D semiconductor nanostructures*, Optics express **20**, 13847 (2012).

[9] C. Bohren and D. Huffman, *Absorption and Scattering of Light by Small Particles*, Wiley, 2008.

[10] Y. Zhan, J. Zhao, C. Zhou, M. Alemayehu, Y. Li, and Y. Li, *Enhanced photon absorption of single nanowire a-Si solar cells modulated by silver core*, Optics express **20**, 158 (2012).

[11] T. Bambino, A. Breitschaft, V. Barbosa, and L. Guimaraes, *Application of semiclassical and geometrical optics theories to resonant modes of a coated sphere*, Journal of the Optical Society of America. A, Optics, image science, and vision **20**, 489 (2003).

[12] E. Palik, *Handbook of Optical Constants of Solids, Vol. 1*, Academic: New York, 1998.

[13] D.-Y. Liu, S.-Y. Ding, H.-X. Lin, B.-J. Liu, Z.-Z. Ye, F.-R. Fan, B. Ren, and Z.-Q. Tian, *Distinctive Enhanced and Tunable Plasmon Resonant Absorption from Controllable AuATCu2O Nanoparticles: Experimental and Theoretical Modeling*, The Journal of Physical Chemistry **116**, 4477 (2012).

[14] Z. Wang, *Transmission Electron Microscopy of Shape-Controlled Nanocrystals and Their Assemblies*, Journal of Physical Chemistry B **104**, 1153 (2000).

[15] E. Vesseur, *Electron Beam Imaging and Spectroscopy of Plasmonic Nanoantenna Resonances*, PhD thesis, Utrecht University, 2011.

[16] F. Garca de Abajo, *Optical excitations in electron microscopy*, Review of Modern Physics **82**, 209 (2010).

[17] L. Novotny and B. Hecht, *Principles of Nano-Optics*, Cambridge University Press, 2006.

Acknowledgements

Many thanks go out to all the people who helped me finish this thesis. First of all, thanks to Erik Garnett for giving me the opportunity to do my bachelors project in his research group at AMOLF and providing me with such an exciting project. I'd also want to thank the rest of the Garnett Research Group: Sebastian Oener, Mohamed Tachikirt, Forrest Bradbury and Beniamino Sciacca -for being so very patient and helpful during optical measurements- and Sander Mann -for providing me with most of theory needed for this thesis and being willing to answer all my endless questions. Also thanks to Benjamin Brenny for helping us go through the CL measurements, and Toon Coenen for providing supporting information on CL. Furthermore, my acknowledgments to the support staff, for helping with the equipment, and finally many thanks go out to Albert Polman, for being my second supervisor.